Simultaneous measurement of strain, temperature and refractive index based on multimode interference, fiber tapering and fiber Bragg gratings

2016 Meas. Sci. Technol. 27 075107

(http://iopscience.iop.org/0957-0233/27/7/075107)

IOP Publishing Measurement Science and Technology
Meas. Sci. Technol. **27** (2016) 075107 (6pp) doi:10.1088/0957-0233/27/7/075107

Simultaneous measurement of strain, temperature and refractive index based on multimode interference, fiber tapering and fiber Bragg gratings

Ricardo Oliveira[1,2], Jonas H Osório[1], Stenio Aristilde[1], Lúcia Bilro[2,3], Rogerio N Nogueira[2] and Cristiano M B Cordeiro[1]

[1] Instituto de Física 'Gleb Wataghin', Universidade Estadual de Campinas, UNICAMP, Brazil
[2] Instituto de Telecomunicações, Pólo de Aveiro, Aveiro, Portugal
[3] I3N – Institute for Nanostructures, Nanomodelling and Nanofabrication—Physics Department, University of Aveiro, Aveiro, Portugal

E-mail: oliveiraricas@av.it.pt

Received 9 March 2016, revised 4 May 2016
Accepted for publication 26 May 2016
Published 15 June 2016

Abstract

We report the development of an optical fiber sensor capable of simultaneously measuring strain, temperature and refractive index. The sensor is based on the combination of two fiber Bragg gratings written in a standard single-mode fiber, one in an untapered region and another in a tapered region, spliced to a no-core fiber. The possibility of simultaneously measuring three parameters relies on the different sensitivity responses of each part of the sensor. The results have shown the possibility of measuring three parameters simultaneously with a resolution of 3.77 $\mu\varepsilon$, 1.36 °C and 5×10^{-4}, respectively for strain, temperature and refractive index. On top of the multiparameter ability, the simple production and combination of all the parts involved on this optical-fiber-based sensor is an attractive feature for several sensing applications.

Keywords: MMI, multimode interference, fiber sensor, fiber Bragg grating

(Some figures may appear in colour only in the online journal)

1. Introduction

Nowadays, optical fiber sensors are widely used to detect physical, chemical and biological parameters. Among the key features of these sensors are their immunity to electromagnetic interference, the capability to resist harsh environments and the ability to multiplex signals.

An interesting optical fiber sensor which has been receiving attention in recent years is the fiber modal interferometer, commonly known as MMI (multimode interference). This device comprises a single-mode–multimode–single-mode (SMS) fiber structure and presents advantages like simplicity of production, high sensitivity [1, 2] and compactness. Therefore, a variety of parameters such as temperature [1, 3], strain [4], refractive index [1, 3], liquid level [5], displacement [6] and vibration [7], have been measured by this fiber-based device. In addition, the combination of different detection schemes has also been reported to discriminate the parameters being measured [8].

On other hand, fiber Bragg gratings (FBGs) are a common device widely used in sensing applications [9]. However, they suffer from the same mutiparameter discrimination problem reported for MMI-fiber-based devices. Therefore, many schemes have also been adopted to discriminate each parameter individually [10, 11].

Due to the inherent advantages of both MMIs and FBGs, the scientific community has recently proposed the combination of both fiber devices to discriminate different parameters. This will allow the simultaneous measurement of: strain and temperature [12–14], strain and curvature [4],

refractive index and temperature [15, 16, 17], and also magnetic field and temperature [18]. However, none of these works have shown the capability to measure three parameters simultaneously.

Nevertheless, simultaneous measurement of strain, temperature and refractive index has been reported using either tilted FBGs [11], long period gratings connected to polarization-maintaining FBGs [19] or etched-core FBGs [10]. However, the refractive index measurement principle adopted for the first case is based on a change of the envelope area of the cladding mode resonances, which may lead to difficulties on the fitting approximation of the lower and upper envelope curves. In the second case, the FBG wavelength shift and reflection power were used to simultaneously detect the three parameters, yet the results concerning the reflection power have revealed both low sensitivity and repeatability. Regarding the last case, the thin etched-fiber diameter (7 μm) can compromise the manipulation of the sensor head in practical applications.

In this work we present a novel optical fiber sensor capable of simultaneously measuring and discriminating three parameters: strain, temperature and refractive index. A singular combination of two FBGs and a no-core fiber (NCF, an all-silica fiber) was used. The FBGs were inscribed in the same fiber (SMF-28), but in two different parts: one in a tapered region and another in an untapered region. A section of an NCF was then spliced between the fiber containing the FBGs and another single-mode fiber (SMF). As each part of the sensor presents different sensitivity responses to the different physical stimuli, it was possible to simultaneously discriminate the three parameters under study.

2. Principle of operation

In order to produce the fiber sensor, a section of an SMF-28 was tapered down with the flame-brushing technique. In this technique the flame is swept along the fiber while it is being stretched, producing a fiber taper that contains a reduction in its cross section. The taper produced is composed of two adiabatic transitions with a uniform waist in the middle with the following dimensions: 50 μm in diameter and 10 mm in length. The taper diameter was chosen in order to provide enough fiber robustness for easy manipulation during the grating inscription and during measurement. After the tapering process, 266 nm UV radiation from a *Quantel Q-Smart 450* was used to inscribe Bragg gratings in the waist of the tapered (50 μm) and untapered fiber (125 μm), through the phase-mask technique. The laser beam has a circular shape with a 6.5 mm diameter and a pulse duration of 5 ns. The phase mask pitch was selected to produce FBGs in the infrared region with enough separation between them, allowing easy discrimination. The laser beam was guided by mirrors and passed through a cylindrical lens ($f = 20$ cm) which was followed by a slit 3 mm in width, used to shape the beam onto the fibers. The FBGs were written under a repetition rate of 10 Hz, with pulse energy of 5 mJ, during a 15 min exposure time. The long inscription time is related to the lower photosensitivity of the fibers, that can be reduced by hydrogen loading prior to the inscription process. The FBGs were produced to be 3 mm in length and with a high enough peak-to-noise level to be detected in reflection.

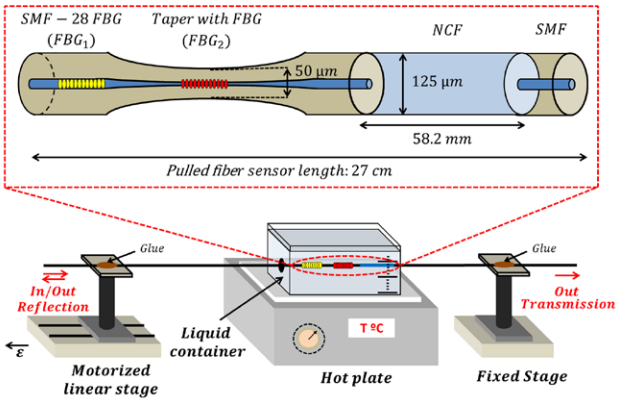

Figure 1. Setup used for the characterization of strain temperature and refractive index. The inset figure shows the sensor structure composed of the combination of two FBGs in untapered and tapered regions of an SMF-28, and an SMS structure containing an NCF.

The second part of the sensor is composed of the SMS structure containing the NCF, which is a pure silica rod with a diameter of 125 μm and with a refractive index of 1.444 at 1550 nm. The complete fiber sensor can be seen in the inset of figure 1. To allow the phenomenon of self-imaging for a specific wavelength in the SMS structure, it is necessary to know the distance at which the input field is replicated, in both amplitude and phase [1]. This length can, therefore, be calculated through

$$L_{\mathrm{NCF}} = \frac{4D_{\mathrm{NCF}}^2 n_{\mathrm{NCF}}}{\lambda}, \tag{1}$$

where n_{NCF} and D_{NCF} are the effective refractive index and diameter of the fundamental mode, respectively; L corresponds to the length of the NCF and λ is related to the peak wavelength.

The calculated length, estimated to have a peak centered at 1550 nm, was thus 58.2 mm. A digital caliper together with a fiber optic cleaver machine were used to cut the NCF at the desired length. The two ends of the NCF were fusion-spliced to an SMF-28 and to the SMF containing the FBGs. To do this, the fibers were inserted in a fiber fusion machine and aligned through the cladding. The NCF was then fusion-spliced to the SMFs and the sensor was ready for the characterization tests.

When changes in strain ($\Delta\varepsilon$), temperature (ΔT) or refractive index (Δn) are applied simultaneously, both parts of the sensor (FBGs and MMI) will react by changing their resonance wavelength. The correspondent wavelength shifts can be expressed by the following matrix:

$$\begin{bmatrix} \Delta\lambda_{\mathrm{FBG\,1}} \\ \Delta\lambda_{\mathrm{FBG\,2}} \\ \Delta\lambda_{\mathrm{NCF}} \end{bmatrix} = \begin{bmatrix} K_{\varepsilon,\mathrm{FBG_1}} & K_{T,\mathrm{FBG_1}} & K_{n,\mathrm{FBG_1}} \\ K_{\varepsilon,\mathrm{FBG_2}} & K_{T,\mathrm{FBG_2}} & K_{n,\mathrm{FBG_2}} \\ K_{\varepsilon,\mathrm{NCF}} & K_{T,\mathrm{NCF}} & K_{n,\mathrm{NCF}} \end{bmatrix} \times \begin{bmatrix} \Delta\varepsilon \\ \Delta T \\ \Delta n \end{bmatrix}, \tag{2}$$

where, $\Delta\lambda_{FBG_1}$ and $\Delta\lambda_{FBG_2}$ represent the wavelength shifts of the FBG in tapered and untapered fiber, respectively; $\Delta\lambda_{NCF}$ denotes the wavelength shift of the NCF; and K_ε, K_T and K_n are the sensitivity coefficients, corresponding to the changes of strain, temperature and refractive index, respectively.

Subscripts FBG_1, FBG_2 and NCF refer to the individual contribution of the FBGs in the untapered/tapered fiber and SMS structure. The three parameters under study can, therefore, be calculated through the equivalent matrix as

$$\begin{bmatrix}\Delta\varepsilon\\ \Delta T\\ \Delta n\end{bmatrix} = \left|M^{-1}\right| \times \begin{bmatrix}\Delta\lambda_{FBG_1}\\ \Delta\lambda_{FBG_2}\\ \Delta\lambda_{NCF}\end{bmatrix}, \tag{3}$$

where M^{-1} is the inverse coefficient matrix.

The wavelength measurement resolution (i.e. $\delta(\Delta\lambda_{FBG_1})$, $\delta(\Delta\lambda_{FBG_2})$ and $\delta(\Delta\lambda_{NCF})$), given by the resolution of the acquisition system, will determine the uncertainty on the measured strain, temperature and refractive index. The correspondent values can be calculated through

$$\begin{bmatrix}\delta(\Delta\varepsilon)\\ \delta(\Delta T)\\ \delta(\Delta n)\end{bmatrix} = \left|M^{-1}\right| \times \begin{bmatrix}\delta(\Delta\lambda_{FBG_1})\\ \delta(\Delta\lambda_{FBG_2})\\ \delta(\Delta\lambda_{NCF})\end{bmatrix}. \tag{4}$$

3. Experimental setup

The experimental setup used to characterize the fiber sensor is shown in figure 1. Both fiber tips were glued to a fixed stage and another to a motorized linear stage (*UTS 150cc*). The distance between the stages where the glue was inserted was 27 cm. On the central region of the setup, a liquid container was placed above a hot plate (*IKA®C-MAG HS7*). The liquid container is used to surround the fiber sensor with a specific refractive index. The hot plate is, therefore, used to control the temperature of the solutions. In order to observe the FBG and SMS spectral responses, an interrogator system (*FS2200—Industrial BraggMETER, FiberSensing*) was used to measure the reflection signal from the FBGs as well as the transmission signal from the SMS structure. The fiber sensor configuration used to measure the reflection signal from the FBGs is presented in figure 1, where the FBG precedes the SMS structure. On other hand, if the opposite configuration is chosen (SMS followed by the FBGs), the FBG reflectivity will be modified by the envelope of the SMS spectra, that is dependent on the external conditions [4, 16]. Therefore, the uncertainty present on the peak wavelength detection with such a configuration could be higher, leading us to exclude this scheme.

The sensor characterization was performed, getting the sensitivity coefficients of each parameter individually: one parameter changes while two others remain constant. For the strain test, the fiber sensor was kept in water, at a constant temperature of 22 °C. The strain was imposed in steps of 92.6 $\mu\varepsilon$ in a range of 1389.0 $\mu\varepsilon$. In order to characterize the sensor to temperature, the liquid container was left with water in it. The temperature was swept from 22–85 °C and no strain was imposed during the tests. For the refractive index tests, the liquid container was filled with six different solutions of water/isopropyl alcohol whose refractive index was previously measured. For each solution, the temperature of the bath was maintained at a constant 22 °C and no strain was imposed on the sensor. The refractive index of the different solutions was measured at 22 °C using a *Palm Abbe®* handheld refractometer with a resolution of 1×10^{-4} and a 590 nm wavelength radiation.

4. Results and discussion

Regarding the results obtained for the FBGs strain test (figures 2(a) and (c)), it can be observed that both FBGs presented a red shift with increasing strain, with values of 5.77 and 0.92 pm $\mu\varepsilon^{-1}$, respectively for the FBG in tapered and untapered fiber. The red shift was expected since the FBGs grating pitch increases with increasing strain.

On other hand, the sensitivities obtained for the untapered and tapered FBGs were decreased and increased respectively, when compared with the value of 1.2 pm $\mu\varepsilon^{-1}$ found for the standard characterization of an FBG written in the same SMF-28. This result is due to the unequal strain distributions along the fiber sensor. The relation between the strain applied in each part of the sensor and the correspondent cross-sectional area can be written as

$$\frac{\varepsilon_{fiber}}{\varepsilon_{taper}} = \frac{A_{taper}}{A_{fiber}}, \tag{5}$$

where ε_{fiber} and ε_{taper} refer to the strain on the fiber and taper, respectively; A_{fiber} and A_{taper} refer to the cross-sectional area of the fiber and taper respectively. Thus, the applied strain will be higher in the tapered region than in the untapered region, since its area is smaller [20]. This leads to a decrease in the sensitivity on the untapered FBG, and to an increase in the tapered FBG [20].

Using the definition of strain and following the deductions given at [20], we can theoretically estimate the sensitivity for the FBG written on the untapered section of the fiber as

$$K_{\varepsilon 1(Theo.)} = K_{\varepsilon(FBG)} \times \frac{L_{FBG_1} + L_{FBG_2} + L_{fiber} + L_{taper}}{L_{taper}\left(\frac{d_{FBG_1}}{d_{taper}}\right)^2 + L_{FBG_2}\left(\frac{d_{FBG_1}}{d_{FBG_2}}\right)^2 + L_{fiber} + L_{FBG_1}}, \tag{6}$$

and for the FBG written on the tapered section as

$$K_{\varepsilon 2(Theo.)} = K_{\varepsilon(FBG)} \times \frac{L_{FBG_1} + L_{FBG_2} + L_{fiber} + L_{taper}}{L_{FBG_1}\left(\frac{d_{FBG_2}}{d_{FBG_1}}\right)^2 + L_{fiber}\left(\frac{d_{FBG_2}}{d_{fiber}}\right)^2 + L_{taper} + L_{FBG_2}} \tag{7}$$

where $K_{\varepsilon(FBG)}$ refers to the strain coefficient of a common FBG written in an SMF28 fiber (1.2 pm $\mu\varepsilon^{-1}$); $L_{(FBG_1)}$, $L_{(FBG_2)}$, $L_{(fiber)}$, and $L_{(taper)}$ are the lengths of each sensor section; d_{FBG_1}, d_{FBG_2}, d_{fiber}, and d_{taper} refer to the diameters of

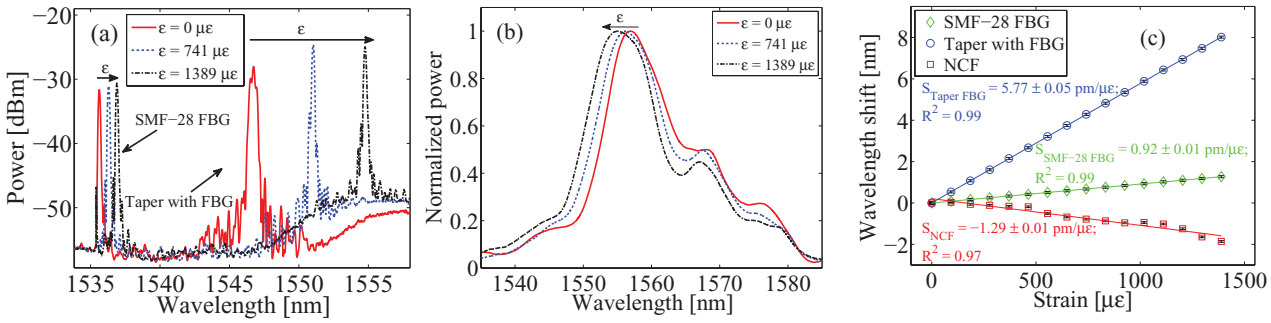

Figure 2. (a) Reflection spectra collected for both FBGs at different strain values; (b) normalized transmission spectra collected for the NCF with different strain values; (c) wavelength shifts from the wavelength peak power for all the parts involved in the sensor at different strain values.

each fiber section. In order to verify the theoretical behavior of both sensitivities presented in equations (6) and (7) for different pulling fiber lengths, we have plotted the two curves on figure 3.

The theoretical values found for the experimental pulling fiber length (27 cm), were 6.33 and 1.01 pm $\mu\varepsilon^{-1}$ for the tapered and untapered fiber, respectively. These theoretical values reveal a close match to the experimental ones, considering that the fiber dimensions used for the theoretical calculation are based on approximated values of the fiber structures and grating dimensions. Additionally, it can be seen from the same figure, that the length of the pulled fiber sensor is also determinant for the FBGs sensitivity, since for longer lengths the effect of the taper section becomes negligible [20].

For the NCF, it can be seen from figures 2(b) and (c), that there was a blue shift with increasing strain, corresponding to a sensitivity of -1.29 pm $\mu\varepsilon^{-1}$. This result is mainly explained by equation (1), since *L*NCF increases and *D*NCF decreases with increasing strain.

Moreover, the unequal strain distribution that occurs on the tapered and untapered section of the SMF-28 will also occur on the NCF fiber, leading to a smaller sensitivity than the theoretical value.

In order to estimate the maximum strain supported by the fiber sensor, we have performed rupture tests for 20 samples with dimensions similar to the ones used in the strain sensitivity measurements. The results show that the tapered region can support maximum strain values that range from half to two times that of the correspondent measured value for the untapered fiber, (10 ± 2) $m\varepsilon$. Moreover, the observed values are comparable to the ones found for a standard single-mode optical fiber, 5.5 $m\varepsilon$, as reported in [21].

Regarding the experimental characterization of the refractive index, the resonant Bragg wavelength for the FBGs does not change with the different solutions (see the data points collected for the Bragg wavelength shifts on figure 4(b)). This result was expected because the fundamental mode on the tapered/untapered regions of the fiber is strongly coupled to the fiber core and, therefore, its evanescent field does not interact with the surrounding medium. On other hand, the NCF presents strong interaction with the surrounding environment (see the spectra change in figure 4(a)). Since the fiber does not present an outer cladding layer, the guided modes can strongly

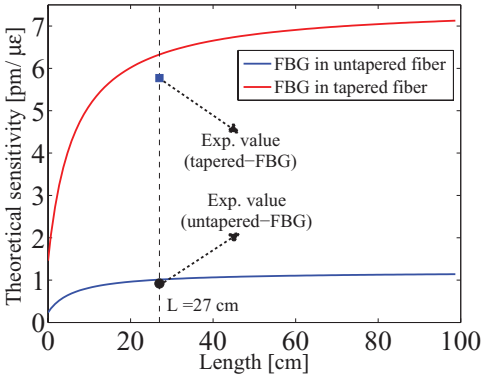

Figure 3. Theoretical FBG strain sensitivity versus total length of the pulling fiber, for the FBG written in the tapered and untapered SMF28.

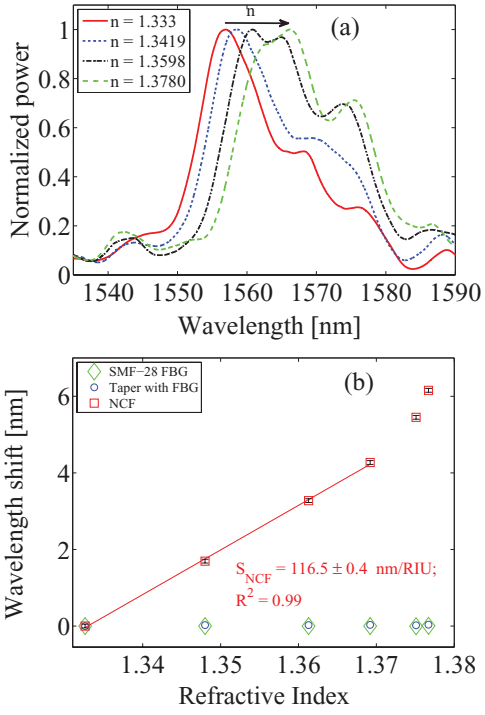

Figure 4. (a) NCF-normalized transmission spectra collected for six different refractive index solutions; (b) wavelength shifts for all the parts involved in the sensor, for different index solutions.

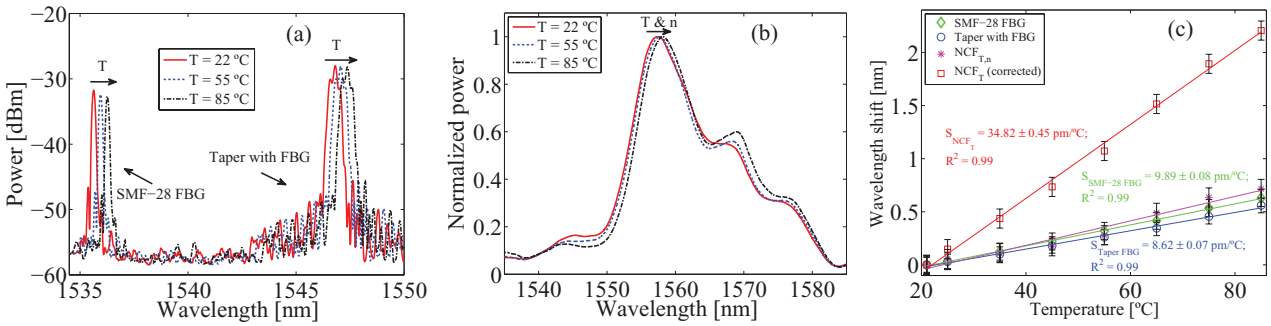

Figure 5. (a) Reflection spectra collected for both FBGs at different temperatures; (b) normalized transmission spectra collected for the NCF with different temperatures, and considering the inherent refractive index change of water; (c) wavelength shifts collected from the wavelength peak power for all the parts involved in the sensor at different temperatures.

interact with the external refractive index solutions. From the different NCF spectra collected, the peak wavelength change was calculated as the center wavelength at 30% of the maximum peak. This was done in order to minimize the uncertainty on the peak wavelength position due to the power transfer that appears between peaks (mainly on the last two spectra of figure 4(a)). The correspondent wavelength shifts were calculated and can be seen in figure 4(b). Additionally, it can be observed that the wavelength shift increases with increasing refractive index and, as expected, the behavior is not linear under the range studied [1, 22]. In order to obtain a linear tendency for the resonant wavelength shifts, a narrow refractive index range (~1.33–1.37) is considered. This range is still valid for several areas of engineering such as environmental sensing; therefore, one can obtain a sensitivity of 116.5 nm RIU^{-1}.

For the temperature characterization, the correspondent spectra change for FBGs and NCF were obtained and can be seen in figures 5(a) and (b)), respectively. From figure 5(c), it can be noticed that the resonance wavelength shifts for the FBGs are similar and positive with increasing temperature. This red shift is mainly due to the thermo-optic coefficient (i.e. change of the refractive index of silica material with temperature). Regarding the results obtained for the NCF (spectra in figure 5(b) and asterisk points on figure 5(c)), it can be seen that there is a red shift of the peak wavelength with increasing temperature. However, this test was done with the fiber sensor immersed in water; therefore, the temperature changes imposed on the characterization test will indirectly induce a change in the refractive index of water [23]. This is not the case with the FBGs since they are wavelength-independent of the external refractive index (figure 4(b)).

Therefore, the NCF wavelength shifts due to the temperature changes alone ($\Delta\lambda_T$), can be calculated as

$$\Delta\lambda_T = \Delta\lambda_{T,n} - K_{n,NCF} \times R_{Water} \times \Delta T, \quad (8)$$

where $\Delta\lambda_{T,n}$ is the overall shift due to the direct and indirect contribution of temperature and water refractive index change, respectively; $K_{n,NCF}$ is the calculated refractive index sensitivity of the NCF (116.5 nm RIU^{-1}); and R_{Water} is the water thermo-optic coefficient, calculated from the data points given in [24] as -2×10^{-4} °C^1. The correspondent $\Delta\lambda_T$ found after the correction can be seen on figure 5(c) as the square points. The correspondent NCF temperature sensitivity was then calculated from the corrected wavelength shifts, giving a value

Table 1. System resolution comparison.

	Proposed sensor	Sensor 1 [19]	Sensor 2 [10]	Sensor 3 [11]
ε ($\mu\varepsilon$)	3.77	7.71	1.96	140.77
T (°C)	1.36	4.02	0.69	15.38
N	5.0×10^{-4}	0.25	9.0×10^{-4}	5.9×10^{-3}

almost four times higher than the ones found for the FBGs. This higher value is probably due to the higher thermo-optic coefficient of the NCF when compared to the SMF-28 [13].

Using the above tests and linear fits, the correspondent $\Delta\varepsilon$, ΔT and Δn, can be simultaneously calculated through

$$\begin{bmatrix} \Delta\varepsilon \\ \Delta T \\ \Delta n \end{bmatrix} = \begin{bmatrix} 0.92 & 9.89 & 0 \\ 5.77 & 8.62 & 0 \\ -1.29 & 34.82 & 116\,500 \end{bmatrix}^{-1} \times \begin{bmatrix} \Delta\lambda_{FBG_1} \\ \Delta\lambda_{FBG_2} \\ \Delta\lambda_{NCF} \end{bmatrix}. \quad (9)$$

The sensor was experimentally tested, giving maximum relative errors of 0.4%, 11% and 8×10^{-4} RIU, respectively, for strain, temperature and refractive index. The differences in the maximum relative errors can be attributed to inaccuracy and uncertainty during the calibration process and also on the peak wavelength detection, especially for the NCF spectra that has a broadened shape. Considering a detection system with a wavelength resolution of 10 pm and using equation (4), the resolution of strain, temperature and refractive index can be calculated respectively as 3.77 $\mu\varepsilon$, 1.36 °C and 5×10^{-4}.

In order to compare the proposed sensor with the ones found in literature, capable of simultaneously detecting strain, temperature and refractive index (i.e. [10, 11, 19], we have constructed a table where we can compare the system resolutions. The values were calculated using equation (4), considering a detection system with a resolution of 10 pm in wavelength and 0.02 dB in amplitude (for sensors based on power (i.e. [11, 19]). The values obtained for sensor 1, presented at [19], were calculated considering a silica fiber Young's modulus of 70 GPa. Additionally, the refractive index value calculated for sensor 3 [11] was calculated individually since this parameter is taken independently from the temperature and strain parameters. The correspondent system resolutions can be seen in table 1.

The values presented in table 1 show that the proposed sensor is well positioned among the different sensors found

in literature, achieving values very close to the ones presented for sensor 2 (i.e. [10]).

The proposed fiber-optic sensor is simply produced due to the easy concatenation of all the parts involved. However, the NCF cleaving process needed to achieve a peak power wavelength centered at the wavelength range of the measurement system needs to be done with special care. This can be easily solved using a learning process.

The capability to simultaneously discriminate strain, temperature and refractive index can be a useful tool; for instance, in the control of the cure processes of materials, where the knowledge of these three parameters is important.

5. Conclusions

We have proposed and demonstrated a simple and effective all-fiber sensor to simultaneously measure strain, temperature and refractive index. The ability to measure different variables without stabilization of the ambient conditions is useful in different areas. The concatenation of the different fiber technologies allows the possibility of simultaneously measuring three parameters with a resolution of 3.77 $\mu\varepsilon$, 1.36 °C and 5×10^{-4}, respectively, for the strain, temperature and refractive index. The simple design and measurement scheme is a highly promising feature for multiparameter sensing applications.

Acknowledgments

This work was funded by FINEP (#01.12.0393.00) and by FCT-Fundação para a Ciência e Tecnologia through Portuguese national funds PEstOE/EEI/LA0008/2013 and UID/EEA/50008/2013 (Swat), PhD Scholarship SFRH/BD/88472/2012, investigator grant IF/01664/2014 and project INITIATE. J H Osório acknowledges CNPq for financial support.

References

[1] Silva S, Pachon E G P, Franco M A R, Hayashi J G, Malcata F X, Frazão O, Jorge P and Cordeiro C M B 2012 Ultrahigh-sensitivity temperature fiber sensor based on multimode interference *Appl. Opt.* **51** 3236–42

[2] Andre R M, Biazoli C R, Silva S O, Marques M B, Cordeiro C M B and Frazao O 2013 Strain-temperature discrimination using multimode interference in tapered fiber *IEEE Photonics Technol. Lett.* **25** 155–8

[3] Chen Y, Han Q, Liu T and Lu X 2015 Self-temperature-compensative refractometer based on singlemode-multimode-singlemode fiber structure *Sensors Actuators* B **212** 107–11

[4] Sun A and Wu Z 2015 Multimode interference in single mode—multimode FBG for simultaneous measurement of strain and bending *IEEE Sensors J.* **15** 3390–4

[5] Antonio-Lopez J E, Torres-Cisneros M, Arredondo-Lucio J A, Sanchez-Mondragon J, Likamwa P and May-Arrioja D A 2010 Novel multimode interference liquid level sensors *Proc. SPIE* **7839** 78391V

[6] Antonio-Lopez J E, LiKamWa P, Sanchez-Mondragon J and May-Arrioja D A 2013 All-fiber multimode interference micro-displacement sensor *Meas. Sci. Technol.* **24** 055104

[7] Ran Y, Xia L, Han Y, Li W, Rohollahnejad J, Wen Y and Liu D 2015 Vibration fiber sensors based on SM-NC-SM fiber structure *IEEE Photonics J.* **7** 6800607

[8] Luo Y, Xia L, Yu C, Li W, Sun Q, Wang Y and Liu D 2015 Multi-parameter optical fiber sensor based on enhanced multimode interference *Opt. Commun.* **344** 120–4

[9] Cusano A, Cutolo A and Albert J 2011 *Fiber Bragg Grating Sensors: Recent Advancements, Industrial Applications and Market Exploitation* (Sharjah: Bentham Science Publishers)

[10] Lee S-M, Saini S and Jeong M 2010 Simultaneous measurement of refractive index, temperature, and strain using etched-core fiber Bragg grating sensors *IEEE Photonics Technol. Lett.* **22** 1431–3

[11] Alberto N J, Marques C A, Pinto J L and Nogueira R N 2010 Three-parameter optical fiber sensor based on a tilted fiber Bragg grating *Appl. Opt.* **49** 6085–91

[12] Li C, Ning T, Wen X, Li J, Zheng J, You H, Chen H, Zhang C and Jian W 2015 Strain and temperature discrimination using a fiber Bragg grating and multimode interference effects *Opt. Commun.* **343** 6–9

[13] Zhou D-P, Wei L, Liu W-K, Liu Y and Lit J W Y 2008 Simultaneous measurement for strain and temperature using fiber Bragg gratings and multimode fibers *Appl. Opt.* **47** 1668–72

[14] Yu S, Pei L, Liu C, Wang Y and Weng S 2014 Simultaneous strain and temperature measurement using a no-core fiber-based modal interferometer with embedded fiber Bragg grating *Opt. Eng.* **53** 087105

[15] Wu Q, Semenova Y, Yan B, Ma Y, Wang P, Yu C and Farrell G 2011 Fiber refractometer based on a fiber Bragg grating and single-mode–multimode–single-mode fiber structure *Opt. Lett.* **36** 2197–9

[16] Li L, Xia L, Wuang Y, Ran Y, Yang C and Liu D 2012 Novel NCF-FBG interferometer for simultaneous measurement of refractive index and temperature *IEEE Photonics Technol. Lett.* **24** 2268–71

[17] Rong Q, Qiao X, Guo T, Wang R, Zhang J, Hu M, Feng Z, Weng Y and Ma Y 2012 Temperature-calibrated fiber-optic refractometer based on a compact FBG-SMS structure *Chin. Opt. Lett.* **10** 030604

[18] Li C, Ning T, Wen X, Li J, Zhang C and Zhang C 2015 Magnetic field and temperature sensor based on a no-core fiber combined with a fiber Bragg grating *Opt. Laser Technol.* **72** 104–7

[19] Mau J, Wu P, Fu M and Liu W 2012 Simultaneous measurement of stress, temperature and refractive index using an PMFBG cascaded with an LPG *Prog. Electromagn. Res. Symp. Proc. (Kuala Lumpur, Malaysia)* pp 1584–8

[20] Frazão O, Silva S F O, Guerreiro A, Santos J L, Ferreira L A and Araújo F M 2007 Strain sensitivity control of fiber Bragg grating structures with fused tapers *Appl. Opt.* **46** 8578–82

[21] Antunes P, Lima H, Monteiro J and Andre P S 2008 Elastic constant measurement for standard and photosensitive single mode optical fibres *Microw. Opt. Technol. Lett.* **50** 2467–9

[22] Biazoli C R, Silva S, Franco M A R, Frazão O and Cordeiro C M B 2012 Multimode interference tapered fiber refractive index sensors *Appl. Opt.* **51** 5941–5

[23] Yan J, Zhang A P, Shao L, Ding J and He S 2007 Simultaneous measurement of refractive index and temperature by using dual long-period gratings with an etching process *IEEE Sensors J.* **7** 1360–1

[24] Lide D R 2004 *CRC Handbook of Chemistry and Physics* (Boca Raton, FL: CRC Press)